Supplementary information

Experimental evidence of an electronic transition in CeP under pressure preceding the volume collapsing isostructural transition using Ce L$_3$–edge x-ray absorption spectroscopy

B. Joseph[1], R. Torchio[2], C. Benndorf[3], T. Irifune[4], T. Shinmei[4], R. Pöttgen[3], A. Zerr[5]

[1]ELETTRA-Sincrotrone Trieste, Strada Statale 14, Km 163.5, Basovizza, Trieste, Italy
[2]European Synchrotron Radiation Facility, BP220, 38043 Grenoble Cedex, France
[3]Institut für Anorganische und Analytische Chemie, Universität Münster, Corrensstrasse 30, 48149, Münster, Germany
[4]Geodynamics Research Center, Ehime University Bunkyo-cho,7908577 Matsuyama, Japan
[5]Laboratoire des Sciences des Procédés et des Matériaux LSPM, CNRS, Université Paris 13, Sorbonne Paris Cité, 93430 Villetaneuse, France

1. CeP synthesis

Since CeP is commercially not available, it was synthesized via a classical ceramic route. The sample of cerium phosphide was prepared directly from the elements using cerium ingots (Smart Elements, purity 99.9 %) and pieces of red phosphorus (ABCR, ultrapure). The cerium was previously turned into filings under dry mineral oil (Na as drying agent) and the red phosphorus was crushed to fine powder under cyclohexane. The elements were mixed in the ideal atomic ratio under cyclohexane and cold-pressed into a pellet of 6 mm diameter. Then the pellet was placed in a pre-calcined corundum crucible and sealed in an evacuated quartz tube, which was subsequently placed in a tube furnace and heated to 673 K in an interval of 12 h. The temperature was increased to 1223 K and kept for 5 d followed by cooling to room temperature over 12 h. The obtained sample was ground to a fine powder under cyclohexane, cold pressed into a pellet again, sealed in a quartz ampoule as described and repeatedly heated to 1223 K for 5 d followed by subsequent cooling to RT. To increase the purity and homogeneity of the cerium phosphide this procedure was repeated five times.

The purity of the sample was checked by X-ray powder diffraction: Guinier technique, Enraf-Nonius FR552 camera (Cu K$_{\alpha 1}$ radiation) equipped with an image plate system (Fujifilm, BAS-1800) using α-quartz (a = 491.30 and c = 540.46 pm) as an internal standard. The CeP sample was pure on the level of powder diffractions. The phosphide was obtained as a moisture-sensitive black powder exuding the smell of phosphine gas and was stored under dry argon atmosphere and/or dry mineral oil to prevent decomposition.

2. CeP high-pressure diffraction
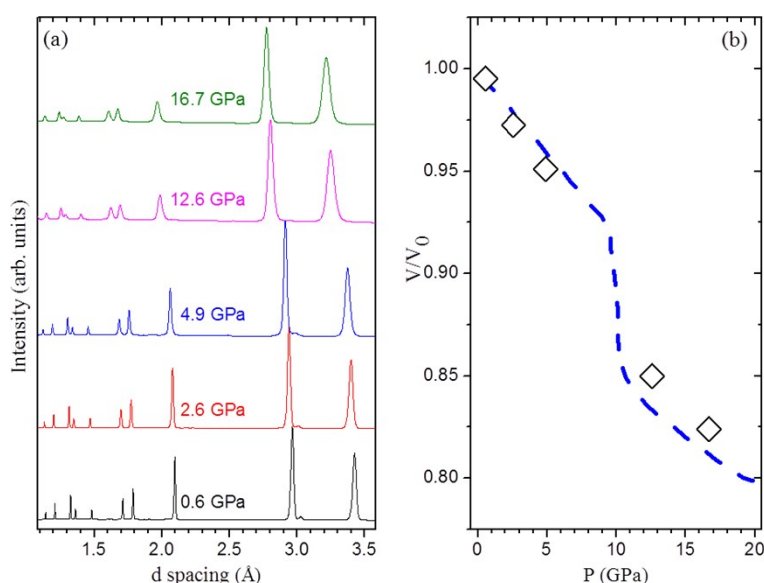
Suppl. Fig. 1: **(a)** XRD patterns of the CeP sample at five different pressure points. **(b)** Normalized unit-cell volume of CeP as a function of pressure from Ref. [1] (dashed line) together with our data points (diamonds) corresponding to the diffraction patterns shown in (a). The error bars for the measured unit-cell volume of CeP are within the symbol size.

Cerium phosphide belongs to the class of rare-earth monopnictides which crystallize with a NaCl type structure where the rare-earth ion is in trivalent state [1]. Among the various fascinating properties of CeP under pressure, the most noted is an isomorphous transition around 10 GPa [1-6]. Although all the earlier structural investigations supported the above mentioned isomorphous transition around 10 GPa, details like the jump in the unit-cell volume, the sharpness of the transition *etc.* varied in the different reports [1-3].These discrepancies may have their origin in a different degree of hydrostaticity of pressure achieved in various experiments or in the relaxation time between each pressure increase and the diffraction measurements. Considering this, we have undertaken a high-pressure X-ray diffraction study of the sample powder, with a limited number of pressure points covering the critical pressure range around 10 GPa, to verify that the crystal structure of CeP remains the same before and after the transition. These measurements were carried out at the newly commissioned high-pressure powder diffraction facility, the Xpress beamline, at the Elettra-Sincrotrone Trieste which provides a higher angular resolution and signal-to-noise ratio when compared with the technique used in the earlier XRD studies at high pressures. Measurements were carried out with silicone oil as the pressure-transmitting medium. Pressure was monitored during the diffraction experiments by ruby fluorescence spectra [7]. During the pressure run, ruby fluorescence spectra did not indicate any significant non-hydrostaticity up to the highest pressure of the work. However, some broadening of the XRD peaks above 10 GPa could be recognized. Results of these investigations are shown in Figure 1 in comparison with the pressure dependent V/V_0 curve from Ref. [1]. As is evident from the XRD pattern shown, CeP maintains in the NaCl-type structure up to 16.7 GPa.

3. Ce L_3–edge XANES curve fitting details

3.1. Four Gaussian peaks fit
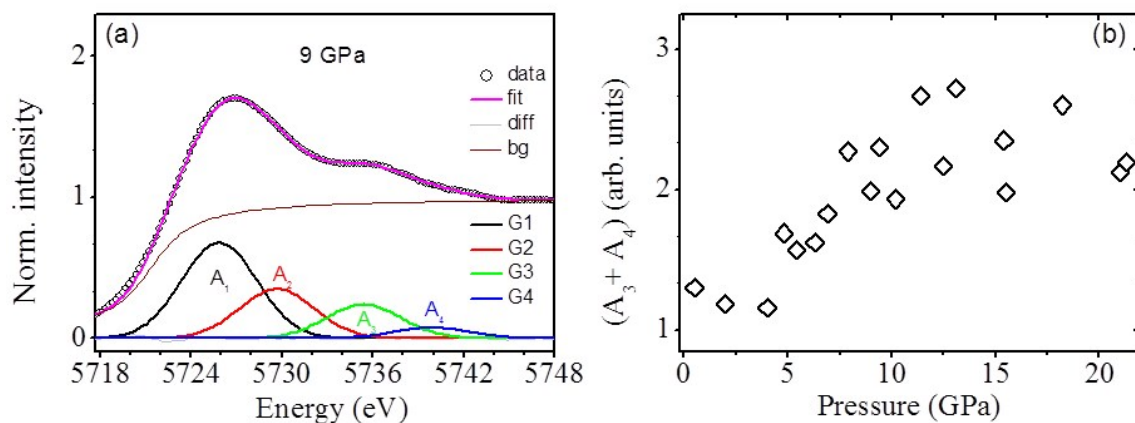
Suppl. Fig. 2: **(a)** Example of the curve-fitting to our XANES data collected at 9 GPa. Legends diff, bg, G1, G2, G3 and G4 stand for difference, background, Gaussian 1, Gaussian 2 Gaussian 3 and Gaussian 4 peak respectively. **(b)** Pressure dependence of the combined area of G3 and G4.
As described in the main text, the electronic structural changes can be quantified from a XANES data spectral deconvolution [8-10]. In Suppl. Fig. 2 (a) we show an example of the spectral deconvolution for P = 9 GPa. Table 1 below provides details about results of the spectral deconvolution for all spectra collected in our work. In the next section we have presented the XANES data obtained separately in the two pressure runs. The changes in the Ce $4f$ electronic state occupation is proportional to the ratio $(A_3+A_4)/\Sigma A_i$ where the A_i indicates the area under the Gaussian peak G_i.

In Suppl. Fig. 2 (b), we present evolution with pressure of the combined areas of the peaks G3 and G3 which show distinct behaviors below and above 10 GPa. The data shown in Suppl. Fig. 2 map changes in the electronic structure of CeP which occur at lower pressure than the iso-structural phase transition. This observation suggests that changes in the electronic structure of CeP trigger the structural transition

Table 1 : Results of the spectral deconvolution of the Ce L_3–edge XANES data measured on pressure increase. Superscript 2 in the first column indicates the second pressure run. For

each spectrum, the curve-fitting was carried out using the Athena software package [11] with two line-shape functions: arctangent for the background fitting (bg) and Gaussian curves for the peaks fitting (G1, G2, G3 and G4). In the arctangent function the width was fixed at 2.12 eV while the edge position e_0 and the step-height h were free parameters. A constant width of 2.5 eV was used for the all Gaussian functions while their peak positions (e_1, e_2, e_3 and e_4) and areas (A_1, A_2, A_3 and A_4) were fitted. The relative change in the Ce $4f$ electronic states is estimated from the ratio of the peak areas ((A_3+A_4)/ΣA_i) and is marked as ($4f^0/(4f^1+4f^0)$) in the last column. Last two rows presents the results of the spectral deconvolution of the Ce^{3+} and Ce^{4+} oxidation standards respectively, CeF_3 and CeO_2. For the standards, the arctangent function width was same as for CeP, while the Gaussian function widths were different and are given below.

P	bg		G1		G2		G3		G4		Sum	Sum	$4f^0/(4f^1+4f^0)$
GPa	e_0 (eV)	h	e_1 (eV)	A_1	e_2 (eV)	A_2	e_3 (eV)	A_3	e_4 (eV)	A_4	A_1+A_2	A_3+A_4	% ± 4.3
0.5^2	5720.81	0.998	5725.84	6.4	5729.52	2.68	5734.75	1.1	5740.00	0.2	10.18	1.3	12.52
2.0	5721.32	0.998	5726.06	7.08	5729.39	2.24	5733.86	1.17	5740.00	0.02	10.49	1.19	11.32
4.0	5721.28	1.000	5726.14	7.14	5730.12	2.26	5734.14	1.13	5735.17	0.03	10.53	1.16	10.98
4.8^2	5721.09	1.000	5725.62	5.48	5729.36	2.91	5734.84	1.32	5739.79	0.37	9.71	1.69	16.77
5.4^2	5721.78	1.000	5725.59	4.42	5729.27	2.60	5734.90	1.20	5739.85	0.37	8.22	1.57	18.28
6.3	5721.20	0.999	5726.21	6.12	5730.11	2.48	5735.02	1.26	5737.72	0.36	9.43	1.62	15.85
6.9^2	5721.08	0.997	5725.81	5.00	5729.62	2.46	5735.13	1.37	5739.91	0.46	7.46	1.83	19.7
7.9	5721.53	0.958	5726.57	5.21	5731.41	1.88	5736.54	1.89	5743.07	0.38	7.09	2.27	24.25
9.0^2	5721.35	1.000	5725.86	4.26	5729.67	2.20	5735.41	1.51	5739.88	0.48	6.46	1.99	23.55
9.4	5721.64	0.950	5726.84	3.67	5731.51	1.31	5736.26	1.87	5741.39	0.43	4.98	2.3	31.59
10.2^2	5721.37	1.000	5726.08	3.48	5729.91	1.59	5735.75	1.51	5740.19	0.42	5.07	1.93	27.57
11.4	5721.93	0.954	5727.06	3.51	5732.29	1.63	5737.00	2.17	5743.64	0.50	5.14	2.67	34.18
12.5	5721.66	0.966	5727.21	3.36	5732.64	1.64	5737.18	1.83	5743.59	0.34	5	2.17	30.26
13.1^2	5721.40	0.980	5726.92	3.79	5732.59	1.75	5737.30	2.22	5743.31	0.50	5.54	2.72	32.93
15.4^2	5721.52	0.978	5727.21	3.34	5733.40	1.81	5737.79	1.91	5744.53	0.44	5.15	2.35	31.33
15.5	5721.71	0.963	5727.67	3.22	5733.65	2.01	5738.02	1.58	5744.60	0.40	5.23	1.98	27.46
18.2^2	5721.85	0.999	5727.14	2.61	5732.56	1.23	5736.91	2.15	5742.17	0.45	3.84	2.6	40.37
21.0^2	5722.09	0.993	5727.43	2.43	5733.78	1.52	5737.71	1.8	5743.14	0.32	3.95	2.12	34.93
21.3	5722.01	0.974	5727.60	2.62	5732.90	1.57	5737.18	1.81	5743.18	0.38	4.19	2.19	34.33
std.													
3+	5719.75	0.978	5727.37	20.7	5731.2	5.95	5740.34	0.15	5741.05	0.38	26.65	0.53	0.02
4+	5724.12	0.953	5727.22	3.32	5731.00	6.51	5737.19	7.23	5741.21	2.0	9.83	9.23	48.4

Gaussian function widths for the Ce^{3+} standard are 1.86, 2.42, 2.5 and 2.5 eV and Gaussian function widths for the Ce^{4+} standard are 2.01, 2.19, 2.6 and 2.75 eV

3.2. Two Gaussian peaks fit
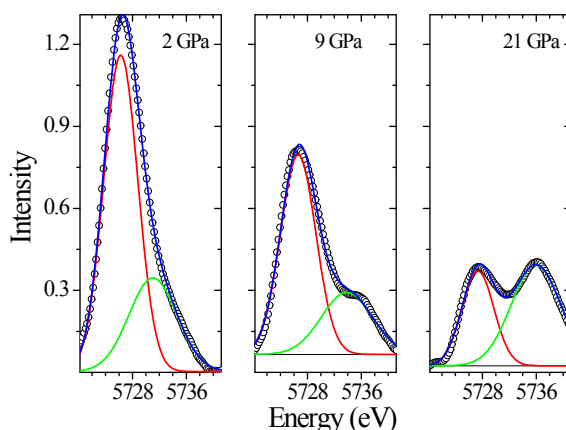
Suppl. Fig. 3: Example of two Gaussian curve-fitting to the background subtracted XANES data of CeP collected at three pressures. Symbols are the data. Blue line is the fit result. Red and green lines represent the two Gaussian functions obtained from the fits.

As described in the main text, we have adopted two kind of curve fitting procedure to quantify changes of the electronic structure of CeP using the Ce L_3 XANES data. First method is described in the main text while the secondis described below: It involves a two Gaussian curve fit to the

background subtracted XANES data where the background is simulated using an arctangent function. Details of the lines shapes and intensities obtained from the fits are given in Table. 2. Examples of the two Gaussian peak fits for the CeP sample at three selected pressures are shown in Suppl. Fig. 3.

Table 2 : Results of the spectral deconvolution of the Ce L_3–edge XANES data of CeP using two Gaussian peaks and an arctangent function. Superscript 2 in the first column indicates the second pressure run. In the arctangent function the width was fixed at 2.12 eV while the edge position e_0 and the step-height h were free parameters. The relative change in the Ce $4f$ electronic states ($4f^0/(4f^1+4f^0)$) is estimated from the ratio of the peak areas ($A_2/(A_1+A_2)$).

P	bg		G1			G2			$A_2/(A_1+A_2)$	$4f^0/(4f^1+4f^0)$
GPa	e_0 (eV)	h	e_1 (eV)	A_1	w1	e_2 (eV)	A_2	w2	%	$\% \pm 4.3$
0.5^2	5720.81	0.998	5726.24	6.63	6.12	5730.94	3.11	9.49	31.92	2.95
2.0	5721.32	0.998	5726.26	7.36	5.98	5731.04	3.07	8.42	29.43	0.46
4.0	5721.28	1.000	5726.34	7.21	6.08	5731.59	3.25	9.31	31.11	2.13
4.8^2	5721.09	1.000	5726.25	5.97	6.26	5731.51	2.95	9.80	33.10	4.13
5.4^2	5721.78	1.000	5726.41	5.30	6.44	5732.30	2.16	9.5	28.97	0
6.3	5721.20	0.999	5726.53	6.51	6.11	5733	2.78	8.9	29.92	0.94
6.9^2	5721.08	0.997	5726.41	5.24	6.13	5732.14	2.60	9.97	33.19	4.22
7.9	5721.53	0.958	5726.8	4.83	5.83	5734.11	3.1	9.13	39.1	10.12
9.0^2	5721.35	1.000	5726.57	4.68	6.13	5733.56	2.3	9.36	32.95	3.98
9.4	5721.64	0.950	5727.04	3.28	5.58	5734.79	2.9	9.02	46.92	17.95
10.2^2	5721.37	1.000	5726.59	3.28	5.68	5733.72	2.3	10.17	41.18	12.21
11.4	5721.93	0.954	5727.27	3.25	5.85	5735.35	3.47	8.75	51.62	22.65
12.5	5721.66	0.966	5727.33	3	5.79	5735.09	3.25	8.85	52.02	23.05
13.1^2	5721.40	0.980	5726.99	3.44	5.89	5735.51	3.97	9.5	53.59	24.61
15.4^2	5721.52	0.978	5727.1	2.82	5.68	5735.49	3.84	9.42	57.68	28.70
15.5	5721.71	0.963	5727.45	2.51	5.59	5734.97	3.95	9.75	61.16	32.18
18.2^2	5721.85	0.999	5727.32	2.33	5.7	5735.86	3.21	8.35	57.97	29.00
21.0^2	5722.09	0.993	5727.34	2.06	5.61	5735.97	3.42	8.69	62.28	33.30
21.3	5722.01	0.974	5727.66	2.19	5.63	5735.19	3.36	8.94	60.50	31.53
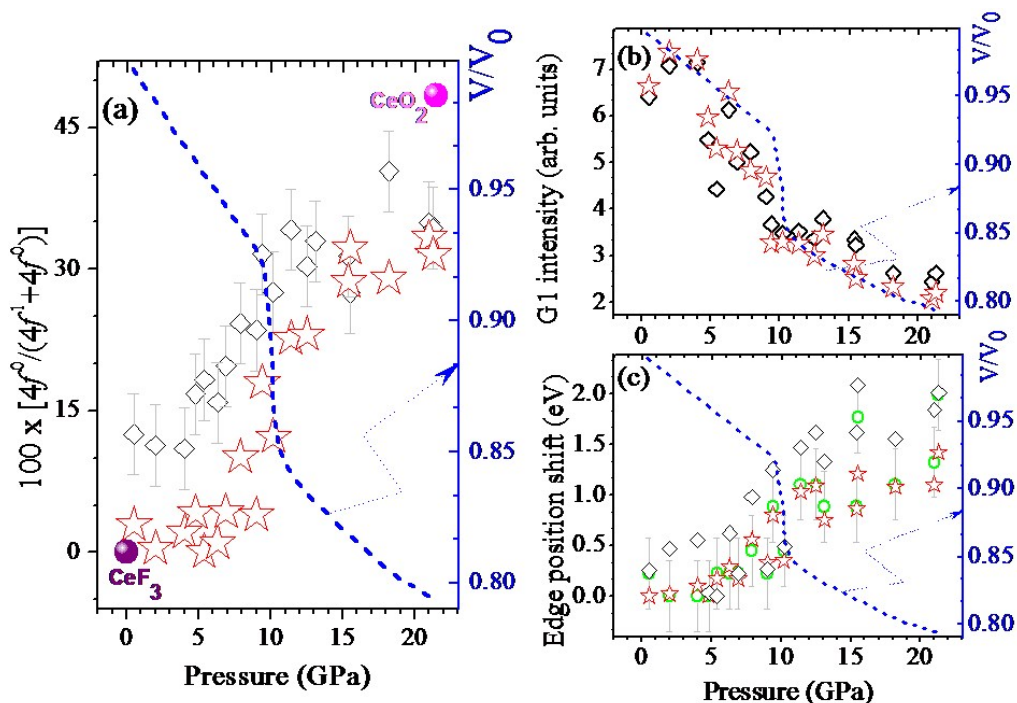
Suppl. Fig. 4: (a) Pressure dependence of the (a) $4f^0$ occupation [$100 \times (4\,f^0/(4\,f^0+4f^1))$] and (b) G1 peak intensity. Symbols, diamonds and stars, represent, respectively, the four and two Gaussian peaks fit procedures. (c) Relative absorption edge position shift obtained from the first derivative spectra (green circles) in comparison with the relative positions of the first Gaussian peak from two peaks (stars) and four peaks (diamonds) deconvolution. In all the cases, the lowest value is taken as

the reference to obtain the relative position shifts. In all panels, the dashed lines indicate the specific volume change of CeP as function of pressure taken from Ref. [1].

4. Ce L$_3$ XANES spectral weight changes

As is the case for normalized XANES data (Suppl. Fig. 5), signal intensity in the pre-edge region (<5714 eV) is close to zero while in the post-edge region (>5748 eV) close to unity. A decrease of the Ce L$_3$-edge whiteline intensity (magenta shaded region) with increasing pressure can be clearly recognised. Appearance of a new peak at higher photon energies around 5737 eV (cyan shaded region) can be also seen in spectra collected at pressures above ~5 GPa. These two features and their change reflect the cerium charge configuration state evolution with compression. In particular, the whiteline intensity is related to the unoccupied 5d valence density of states and a decrease of its intensity indicates increasing occupation of the 5d electronic states due to a delocalization of the valence electrons.
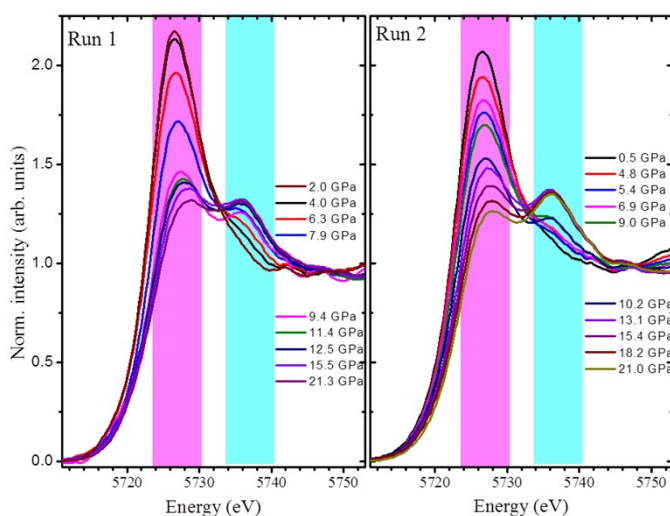
Suppl. Fig. 5: Normalized XANES data for pressure runs 1 and 2 (left and right panels, respectively). The shaded regions indicate the photon energy regions where the spectral weights were determined by integrating the area under the curve.
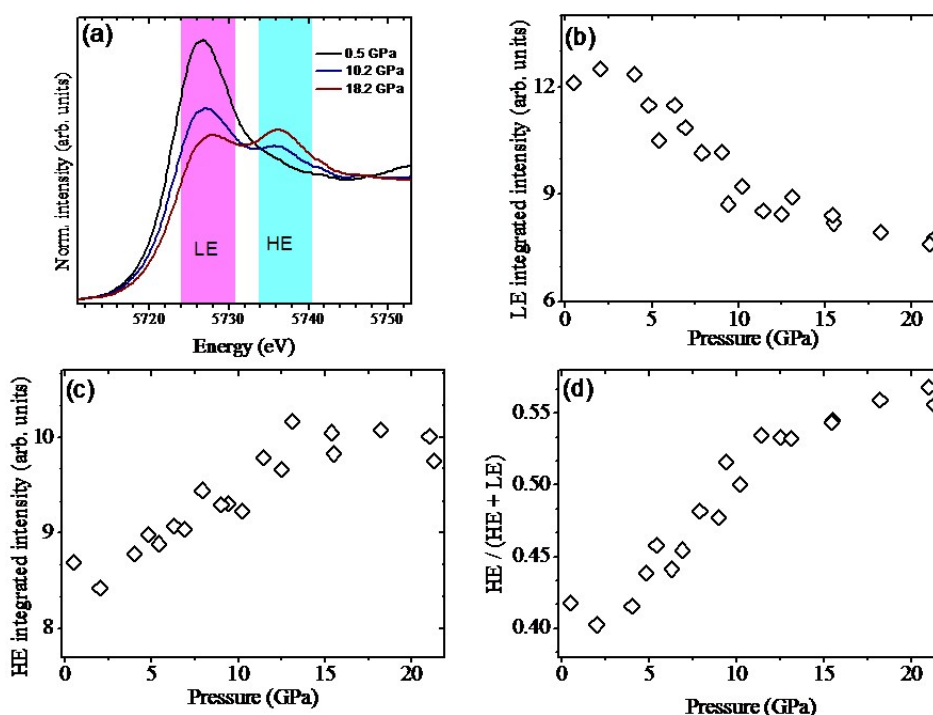
Suppl. Fig. 6 (a): Examples of normalized XANES spectra of CeP at three pressures which show clearly the intensity redistribution between the low energy (LE) and high energy (HE) regions of the

spectra. **(b)** and **(c)** show pressure dependences of the integrated peak intensities in the LE- and HE-energy region, respectively. **(d)** represents pressure dependence of the ratio A_{HE}/A_{LE+HE}.

In Suppl. Fig. 6. we present the integrated signal intensity in the shaded photon energy regions with the aim to quantify in an alternative manner the pressure dependence. A decrease in the Ce L_3-edge whiteline intensity (LE, magenta shaded region) with pressure is readily seen in Suppl. Fig. 6 (b). There are only minimal changes of the integrated intensities at the low pressures, however close to 9 GPa, there is a rather steep change which is followed by a constant regime at the high pressures These dependences underline the changes the 4f electronic configuration of the CeP system.

4. Reversibility of the electronic and structural transitions

We have verified in this work that both the isostructural phase transition at ~10 GPa and the correlated electronic transformation in CeP above ~5 GPa are reversible. This can be clearly appreciated from the data collected on pressure increase and decrease shown in Suppl. Fig. 7(a) and (b).
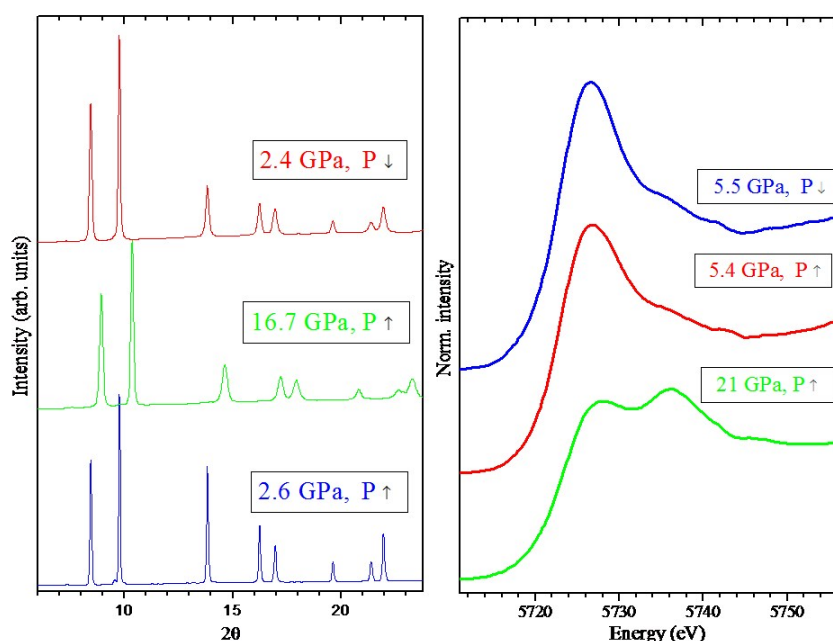
Suppl. Fig. 7 (a): X-ray diffraction patterns of CeP collected on pressure increase at 2.6 GPa and 16.7 GPa compared with that collected upon the subsequent decompression to 2.4 GPa. **(b)** Ce L_3 XANES data of CeP at 5.4 GPa and 21 GPa measured upon pressure increase in comparison with the spectrum obtained after the subsequent pressure decrease to 5.5 GPa. The latter spectrum (at 5.5 GPa) exhibits the same features as the spectrum collected on pressure increase at 5.4 GPa.

References:

1   A. Jayaraman, W. Lowe, L. D. Longinotti, E. Bucher, *Phys. Rev. Lett.* **36**, 367 (1976)
2   I. Vedel, A. M. Redon, J. Rossat-Mignod , O. Vogt, J. M. Leger, *J. Phys. C: Solid State Phys.* **20**, 3439 (1987)
3   N. Ishimatsu, Y. Ohishi, M. Takata, E. Nishibori, M. Sakata, J. Hayashi, I. Shirotani, O. Shimomura, *J. Phys.: Condens. Matter* **14**, 11143 (2002)
4   A. Svane, Z. Szotek, W. M. Temmerman, J. Laegsgaard, H. Winter, *J. Phys.: Condens. Matter* **10**, 5309 (1998)
5   A. Svane, Z. Szotek, W. M. Temmerman, J. Laegsgaard, H. Winter, *Phys. Stat. Sol. B* **223**, 105 (2001)
6   V. Srivastava, A. K. Bandyopadhyay, P. K. Jha, S. P. Sanyal, *J. Phys. Chem. Solids.* **64**, 907 (2003)
7   H. K. Mao, P. M. Bell, J. W. Shaner, and D. J. Steinberg, *J. Appl. Phys.* **49**, 3276 (1978).
8   T. Sugimoto, B. Joseph, E. Paris, A. Iadecola, T. Mizokawa, S. Demura, Y. Mizuguchi, Y. Takano, N. L. Saini, *Phys. Rev. B* **89**, 201117 (2014)
9   A. Bianconi, A. Marcelli, H. Dexpert, R. Karnatak, A. Kotani, T. Jo and J. Petiau, *Phys. Rev. B* **35**, 806 (1987)
10 N. M. Souza-Neto, D. Haskel, R. D. Dos Reis, F. C. G. Grandra, *High Pressure Research* **36**, 360 (2016)
11 B. Ravel, M. Newville, *J. Synchrotron Rad.* **12**, 537 (2005)